
Social Processes: Self-Supervised Forecasting of Nonverbal Cues in Social Conversations

Chirag Raman

Hayley Hung

Marco Loog

Delft University of Technology, Delft, The Netherlands
{c.a.raman, h.hung, m.loog}@tudelft.nl

Abstract

The default paradigm for the forecasting of human behavior in social conversations is characterized by top-down approaches. These involve identifying predictive relationships between low level nonverbal cues and future semantic events of interest (e.g. turn changes, group leaving). A common hurdle however, is the limited availability of labeled data for supervised learning. In this work, we take the first step in the direction of a bottom-up self-supervised approach in the domain. We formulate the task of Social Cue Forecasting to leverage the larger amount of unlabeled low-level behavior cues, and characterize the modeling challenges involved. To address these, we take a meta-learning approach and propose the Social Process (SP) models—socially aware sequence-to-sequence (Seq2Seq) models within the Neural Process (NP) family. SP models learn extractable representations of non-semantic future cues for each participant, while capturing global uncertainty by jointly reasoning about the future for all members of the group. Evaluation on synthesized and real-world behavior data shows that our SP models achieve higher log-likelihood than the NP baselines, and also highlights important considerations for applying such techniques within the domain of social human interactions.

1 Introduction

Picture a situated interactive agent such as a social robot conversing with a group of people. How can agents act in such a setting? We sustain conversations spatially and temporally through explicit behavioral cues—examples include locations of partners, their orientation, gestures, gaze, and floor control actions [1–3]. Evidence suggests that we employ an anticipation of these and other cues to navigate daily social interactions [1, 4–8]. Consequently, the ability to forecast the future constitutes a natural objective towards the realization of machines with social skills. As such, interactive agents typically contend with uncertainties in inferences surrounding cues [3]. So beyond making real-time inferences, such systems may achieve more fluid interactions by leveraging the ability to forecast future states of the conversation [9].

In addition to the development of social agents, behavior forecasting is also of significance in social psychology, where the focus is on gaining insight into human behavior. Since human-interpretability is of essence, top-down approaches largely constitute the default paradigm, where specific events of semantic interest are selected first for consideration and their relationship to potentially predictive cues are studied in isolation—either in controlled interactions in lab settings, or in subsequent statistical analyses [10, 11]. Examples of such semantic events include speaker turn transitions [5, 12, 13], mimicry episodes [14], or the termination of an interaction [9, 15]. However, one hurdle in the top-down paradigm is limited data. The events (that constitute the labels or the dependent variables) often occur infrequently over a longer interaction, reducing the effective amount of labeled data. This precludes the use of neural supervised learning techniques that tend to be data intensive.



Figure 1: Conceptual illustration of forecasting approaches on an in-the-wild conversation from the Match-NMingle dataset [16]. **a.** The top-down approach entails predicting a semantic event or action of interest for the observed window $t_{\text{obs}} := [o1 \dots oT]$. Here we illustrate *group leaving* [15]; the circled individual in the center leaves a group in the future. **b.** In contrast, we propose a bottom-up approach in the social conversation forecasting domain through the task of *Social Cue Forecasting*. This entails using the non-semantic low-level cues over t_{obs} to regress the same cues over the future window $t_{\text{fut}} := [f1 \dots fT]$. In this example we depict the cues of head pose (solid normal), body pose (hollow normal), and speaking status (speaker in orange). The hypothetical uncertainty estimates over t_{fut} are also depicted as shaded spreads.

In this work, we take an initial step towards a bottom-up approach to forecasting human behavior for free standing conversational groups. Our guiding motivation is to learn predictive representations of general future social behavior by utilizing unlabeled streams of low-level behavioral features. We do this by regressing future sequences of these features from observed sequences of the same features in a self-supervised manner. We term this task of non-semantic future behavior forecasting as *Social Cue Forecasting* (SCF).

Our approach is built on the observation that the *social signal* [17]—the high-level attitudes and social meaning transferred in interactions—is already embedded in the low-level cues [18]. To conceptually illustrate the contrasting top-down and bottom-up approaches on an example task, Figure 1 depicts an instance of a group leaving event in a naturalistic social conversation. Evidence suggests that such events can be anticipated from certain preceding *rituals* [15] reflected in the postural changes of conversing members [1]. van Doorn [15] built a predictor using 200 instances of group leaving found in over 90 minutes of mingling interaction and hand-crafted features. In contrast, our bottom-up approach would entail learning task agnostic representations of future behavior using the entire 90 minutes of data, and then training simpler predictors for group leaving using the learnt representations as input. The figure also illustrates the complexity of naturalistic interactions where cross-group social influence exists. In this work we focus on the simpler setting of a single group in a scene.

There are several challenges intrinsic to computationally modeling future behavior in social conversations. The future is intrinsically uncertain, the forecasts for interaction partners are inter-dependent, and the social dynamics is unique for each grouping of individuals. We address these through the following contributions:

- We formalize the task of SCF. We characterize the modeling challenges involved, and cast the problem into the meta-learning paradigm, allowing for data-efficient generalization to unseen groups at evaluation without learning group-specific models.
- We propose and evaluate two socially aware Sequence-to-Sequence (Seq2Seq) models within the Neural Process (NP) family [19] for SCF in social conversations. Our method encodes complex social dynamics informative of future group behavior into extractable representations for each individual.

This paper is organized as follows. In Section 2 we formally define and characterize the task of SCF. We situate this work within broader literature in Section 3, and review background concepts in Section 4. We propose the Social Process models in Section 5 and describe our experiments in Section 6, concluding with a discussion of our findings in Section 7.

2 Social Cue Forecasting

The objective of SCF is to predict future behavioral cues of *all* people involved in a social encounter given an observed sequence of their behavioral features. More formally, let us denote a window

of observed timesteps as $\mathbf{t}_{\text{obs}} := [o1, o2, \dots, oT]$, and an unobserved future time window as $\mathbf{t}_{\text{fut}} := [f1, f2, \dots, fT]$, $f1 > oT$. Note that \mathbf{t}_{fut} and \mathbf{t}_{obs} are typically non-overlapping, can be of different lengths, and \mathbf{t}_{fut} need not immediately follow \mathbf{t}_{obs} . Given a set of n interacting participants, let us denote their social cues over a \mathbf{t}_{obs} and \mathbf{t}_{fut} respectively as

$$\mathbf{X} := [\mathbf{b}_t^i; t \in \mathbf{t}_{\text{obs}}]_{i=1}^n, \quad \mathbf{Y} := [\mathbf{b}_t^i; t \in \mathbf{t}_{\text{fut}}]_{i=1}^n. \quad (1a, b)$$

The vector \mathbf{b}_t^i encapsulates the multimodal cues of interest from participant i at time t . These can include head and body pose, speaking status, facial expressions, gestures, and verbal content—any information stream that combine to transfer social meaning.

In its simplest form, given an \mathbf{X} , the objective of SCF is to learn a single function f such that $\mathbf{Y} = f(\mathbf{X})$. However, an inherent challenge in forecasting behavior is that an observed sequence of interaction does not have a deterministic future and can result in multiple socially valid ones—a window of overlapping speech between people both may and may not result in a change of speaker [12, 20], a change in head orientation may continue into a sweeping glance across the room or a darting glance stopping at a recipient of interest [21]. In some cases certain observed behaviors—intonation and gaze cues [5, 13] or synchronization in speaker-listener speech [22] for turn-taking—might make some outcomes more likely than others. Given that there are both supporting and challenging arguments for how these observations influence subsequent behaviors [22, p. 5; 13, p. 22], it would be beneficial if a data-driven model expresses a measure of uncertainty in its forecasts. We do this by modeling the distribution over possible futures $p(\mathbf{Y}|\mathbf{X})$ rather than forecasting a single future.

Another design consideration arises from a defining characteristic of focused interactions—the participants’ behaviors are interdependent. Participants in a group sustain equal access to the shared interaction space through cooperative maneuvering [1, p. 220]. Moreover, when multiple groups are co-located, outsiders unengaged in these intra-group maneuvers may also influence the behavior of those within the group [23, p. 91; 1, p. 233], sometimes causing them to leave (see Figure 1). It is therefore essential to capture uncertainty in forecasts at the *global* level—jointly forecasting one future for all participants at a time, rather than at a *local* output level—one future for each individual independent of the remaining participants’ futures.

How participants coordinate their behaviors is a function of several individual factors [24, Chap. 1; 1, p. 237]. Consequently, the social dynamics guiding an interaction also has unique attributes for every unique grouping of individuals. Rather than learning group-specific models to capture these unique dynamics, we formulate the forecasting problem in terms of meta-learning, or *few-shot* function estimation. We interpret each unique group of individuals as the meta-learning notion of a task. The core idea is that we can learn to predict a distribution over futures for a target sequence \mathbf{X} having captured the group’s unique behavioral tendencies from a context set C of their observed-future sequences. We can then generalize to unseen groups at evaluation by conditioning on a short observed slice of their interaction. We believe that this approach is especially suitable for social conversation forecasting—a setting that involves a limited data regime where good uncertainty estimates are desirable. Note that when conditioning on context is removed ($C = \emptyset$), we simply revert to the formulation $p(\mathbf{Y}|\mathbf{X})$.

3 Related Work

Free-standing conversations are an example of what social scientists call *focused interactions*, said to arise when a “group of persons gather close together and openly cooperate to sustain a single focus of attention, typically by taking turns at talking” [23, p. 24]. A long-standing topic of study has been the systematic organization of turn-taking [25–27], with a particular interest in the event of upcoming speaking turns [5–8]. There has also been some interest in the forecasting task itself, to anticipate disengagement from an interaction [9, 15], the splitting or merging of groups [28], the time-evolving size of a group [29] or semantic social action labels [30, 31]. Most of these works use heuristics, either to generate semantic labels [9], model the dynamics itself [29], or hand-craft features [15].

Although not a forecasting task, the closest work that shares our motivation in predicting non-semantic low-level features is the recently introduced task of Social Signal Prediction (SSP) [32]. The objective is to predict the social cues¹ of a target person using cues from the communication partners as

¹In the domain of Social Signal Processing, a *social signal* [17] refers to the relational attitudes displayed by people. It is a high-level construct resulting from the perception of cues (see Fig. 1 in [18]). From this

input (Joo et al. focus on predictions within the same time window [32, Eq. 6]). While the most general formulation of SSP involves forecasting a single timestep for a target person given the entire group’s past behavior [32, Eq. 3], generalizing this formulation runs into an inherent problem; applying the definition to forecasting entails iteratively treating each individual as target, learning separate functions for every person. However, as we discuss in Section 2, these futures of interacting individuals are not independent given observed group behavior. Furthermore, a constrained definition of forecasting that predicts an immediate step into the future is limiting, since forecasting an event that occurs after a delay (e.g. a time lagged synchrony [33] or mimicry [14] episode) might be of interest. Operationalizing this definition would entail a sliding window iteratively using predictions over the offset between t_{obs} and t_{fut} as input, which would cascade prediction errors.

A related social setting where forecasting has been of interest is that of *unfocused interactions*. These occur when individuals find themselves by circumstance in the immediate presence of each other, such as pedestrians walking in proximity. Early approaches for forecasting pedestrian trajectories were heuristic based, involving hand-crafted energy potentials to describe the influence pedestrians have on each other [34–41]. More recent approaches encode the relative positional information directly into a neural architecture [42–46].

In a broad sense, the self-supervised learning aspects of this work has some overlap with recent approaches focusing on the non-interaction task of visual forecasting. These works have taken a non-semantic approach to predict low level pixel-based features or intermediate representations [38, 47–52], and demonstrated a utility of the learned representation for other tasks like semi-supervised classification [53], or training agents in immersive environments [54].

4 Preliminaries

Meta-learning. A supervised learning algorithm can be viewed as a function mapping a dataset $C := (\mathbf{X}_C, \mathbf{Y}_C) := \{(\mathbf{x}_i, \mathbf{y}_i)\}_{i \in [N_C]}$ to a predictor $f(\mathbf{x})$. Here N_C is the number of datapoints in C , and $[N_C] := \{1, \dots, N_C\}$. The key idea of meta-learning is to learn the learning process itself, modeling this function representing the initial algorithm using another supervised learning algorithm; hence the name *meta-learning*. In meta-learning literature, a *task* refers to each dataset in a collection $\mathcal{M} := \{\mathcal{T}_i\}_{i=1}^{N_{\text{tasks}}}$ of related datasets [55]. For each task \mathcal{T} , a meta-learner is episodically trained to fit a subset of target points $D := (\mathbf{X}, \mathbf{Y}) := \{(\mathbf{x}_i, \mathbf{y}_i)\}_{i \in [N_D]}$ given another subset of context observations C . At meta-test time, the resulting predictor $f(\mathbf{x}, C)$ uses the information obtained during meta-learning to make predictions for unseen target points conditioned on context sets unseen at meta-training.

Neural Processes Sharing the same core motivations, NPs are a family of latent variable models that extend the idea of meta-learning to situations where uncertainty in the predictions $f(\mathbf{x}, C)$ are desirable. They do this by meta-learning a map from datasets to stochastic processes, estimating a distribution over the predictions $p(\mathbf{Y}|\mathbf{X}, C)$. To capture this distribution, NPs model the conditional latent distribution $p(\mathbf{z}|C)$ from which a task representation $\mathbf{z} \in \mathbb{R}^d$ is sampled. This constitutes the model’s *latent* path. The context can also be incorporated through a *deterministic* path, via a representation $\mathbf{r}_C \in \mathbb{R}^d$ aggregated over C . An observation model $p(\mathbf{y}_i|\mathbf{x}_i, \mathbf{r}_C, \mathbf{z})$ then fits the target observations in D . The generative process for the NP is written as

$$p(\mathbf{Y}|\mathbf{X}, C) := \int p(\mathbf{Y}|\mathbf{X}, C, \mathbf{z})p(\mathbf{z}|C)d\mathbf{z} = \int p(\mathbf{Y}|\mathbf{X}, \mathbf{r}_C, \mathbf{z})q(\mathbf{z}|\mathbf{s}_C)d\mathbf{z}, \quad (2)$$

where $p(\mathbf{Y}|\mathbf{X}, \mathbf{r}_C, \mathbf{z}) := \prod_{i \in [N_D]} p(\mathbf{y}_i|\mathbf{x}_i, \mathbf{r}_C, \mathbf{z})$. The latent \mathbf{z} is modeled by a factorized Gaussian parameterized by $\mathbf{s}_C := f_s(C)$, with f_s being a deterministic function invariant to order permutation over C . When the conditioning on context is removed ($C = \emptyset$), we have $q(\mathbf{z}|\mathbf{s}_\emptyset) := p(\mathbf{z})$, the zero-information prior on \mathbf{z} . C is encoded on the deterministic path using a function f_r similar to f_s , so that $\mathbf{r}_C := f_r(C)$. In practice this is implemented as $\mathbf{r}_C = \sum_{i \in [N_C]} \text{MLP}(\mathbf{x}_i, \mathbf{y}_i)/N_C$. The observation model is referred to as the *decoder*, and q, f_r, f_s comprise the *encoders*. The parameters of the NP are learned for random subsets C and D by maximizing the evidence lower bound (ELBO)

$$\log p(\mathbf{Y}|\mathbf{X}, C) \geq \mathbb{E}_{q(\mathbf{z}|\mathbf{s}_D)}[\log p(\mathbf{Y}|\mathbf{X}, C, \mathbf{z})] - \mathbb{KL}(q(\mathbf{z}|\mathbf{s}_D)||q(\mathbf{z}|\mathbf{s}_C)). \quad (3)$$

perspective, the task of Social Signal Prediction [32] is a misnomer since it still relates to the prediction of cues and not signals, a distinction we preserve in this work.

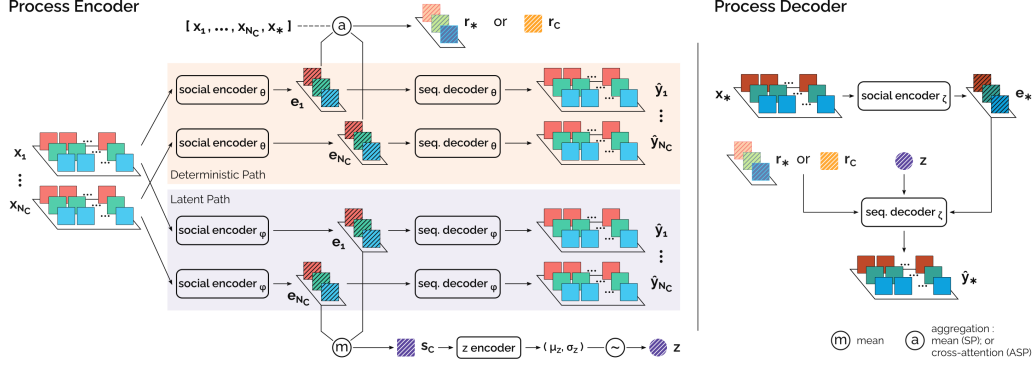


Figure 2: Architecture of the SP and ASP family.

5 Social Processes

In this section we present our socially aware Seq2Seq models within the NP family that is agnostic to group member identities and group size. To setup the task, we split the contextual interaction on which we condition into pairs of observed and future sequences, writing the context as $C := (\mathbf{X}_C, \mathbf{Y}_C) := (\mathbf{X}_j, \mathbf{Y}_k)_{(j,k) \in [N_C] \times [N_C]}$, where every \mathbf{X}_j occurs before the corresponding \mathbf{Y}_k . As discussed in Section 3, domain experts focusing on behavior analysis might be interested in settings where t_{obs} and t_{fut} are offset by an arbitrary delay. Consequently, the j th t_{obs} can have multiple associated t_{fut} windows. Denoting the set of target window pairs as $D := (\mathbf{X}, \mathbf{Y}) := (\mathbf{X}_j, \mathbf{Y}_k)_{(j,k) \in [N_D] \times [N_D]}$, our focus in the rest of this work is to model the distribution $p(\mathbf{Y}|\mathbf{X}, C)$.

The generative process for our model we call the Social Process (SP) follows Eq. 2, which we extend to social forecasting in two ways. We embed an observed sequence \mathbf{x} for an individual into a condensed encoding $\mathbf{e} \in \mathbb{R}^d$ that is then decoded into the future sequence using a Seq2Seq architecture [56, 57]. Our intuition is that this would cause the representation to encode *temporal* information about the future. Further, for every individual we model this \mathbf{e} as a function of their own behavior, and that of their partners as viewed by them. The intuition is that this captures the *spatial* influence partners have on the participant over the t_{obs} . Using notation we established in Section 2, we define the observation model for the SP for a single participant p_i as

$$p(\mathbf{y}^i | \mathbf{x}^i, C, \mathbf{z}) := p(\mathbf{b}_{f1}^i, \dots, \mathbf{b}_{fT}^i | \mathbf{b}_{o1}^i, \dots, \mathbf{b}_{oT}^i, C, \mathbf{z}) = p(\mathbf{b}_{f1}^i, \dots, \mathbf{b}_{fT}^i | \mathbf{e}^i, \mathbf{r}_C, \mathbf{z}). \quad (4)$$

If decoding is carried out in an auto-regressive manner, we can further write the right hand side of Eq. 4 as $\prod_{t=f1}^{fT} p(\mathbf{b}_t^i | \mathbf{b}_{t-1}^i, \dots, \mathbf{b}_{f1}^i, \mathbf{e}^i, \mathbf{r}_C, \mathbf{z})$. Following the standard NP setting, we implement the observation model as a set of Gaussian distributions factorized over time and feature dimensions. We also incorporate the cross-attention mechanism from the Attentive Neural Process (ANP) [58] to define the variant Attentive Social Process (ASP). Following Eq. 4 and the definition of the ANP, the corresponding observation model of the ASP for a single participant is defined as

$$p(\mathbf{y}^i | \mathbf{x}^i, C, \mathbf{z}) = p(\mathbf{b}_{f1}^i, \dots, \mathbf{b}_{fT}^i | \mathbf{e}^i, \mathbf{r}^*(C, \mathbf{x}^i), \mathbf{z}). \quad (5)$$

Here each target query sequence \mathbf{x}_*^i attends to the context sequences \mathbf{X}_C to produce a query-specific representation $\mathbf{r}_* := \mathbf{r}^*(C, \mathbf{x}_*^i) \in \mathbb{R}^d$. The model architectures are illustrated in Figure 2.

Encoding Partner Behavior. While a typical Seq2Seq setup involves conditioning the decoding on solely a compact representation of the observed sequence, we’d like to condition an individual’s forecast on the observed behavior of both, themselves and their partners. We do this using a pair of sequence encoders: one to encode the temporal dynamics of participant p_i ’s features, $\mathbf{e}_{\text{self}}^i = f_{\text{self}}(\mathbf{x}_i)$, and another to encode the dynamics of a transformed representation of the features of p_i ’s partners, $\mathbf{e}_{\text{partner}}^i = f_{\text{partner}}(\psi(\mathbf{x}_{j, (j \neq i)}))$. Using a separate network to encode partner behavior grants the practical advantage of being able to sample an individual’s and partners’ features at different sampling rates.

How do we model $\psi(\mathbf{x}_j)$? We want the partners’ representation to possess two properties: *permutation invariance*—changing the order of the partners should not affect the representation; and *group size independence*—we want to compactly represent all partners independent of the group size.

Beyond coordinate space invariance, we wish to intuitively capture a view of the interaction from p_i 's perspective. We extend the approach Qi et al. [59] applied to point clouds to focused interactions by computing pooled embeddings of relative behavioral features. Since most commonly considered nonverbal cues in literature (see Section 6.3) include the attributes of orientation or location (e.g. head/body pose or keypoints) or a binary indicator (such as speaking status), we specify how we transform these. The 3D pose (orientation, location) of every partner p_j is transformed to a frame of reference defined by p_i 's pose. At timestep t , denoting orientation, location, and binary speaking status for p_i as $\mathbf{b}_t^i = [\mathbf{q}^i; \mathbf{l}^i; s^i]$, and those for p_j as $\mathbf{b}_t^j = [\mathbf{q}^j; \mathbf{l}^j; s^j]$, we have

$$\mathbf{q}^{rel} = \mathbf{q}^i * (\mathbf{q}^j)^{-1}, \quad \mathbf{l}^{rel} = \mathbf{l}^j - \mathbf{l}^i, \quad s^{rel} = s^j - s^i. \quad (6a-c)$$

Note that we use unit quaternions (denoted \mathbf{q}) for representing orientation due their various benefits over other representations of rotation [60, Sec. 3.2]. The operator $*$ denotes the Hamilton product of the quaternions. These transformed features for each p_j are encoded using an *embedder* MLP. The outputs are concatenated with \mathbf{e}_{self}^j and processed by a *pre-pooler* MLP, which is followed by the symmetric element-wise Max-pooling function to obtain $\psi(\mathbf{x}^j)$ at each timestep. We capture the dynamics in the pooled representation over \mathbf{t}_{obs} using $f_{partner}$. Finally, we combine \mathbf{e}_{self}^i and $\mathbf{e}_{partner}^i$ for p_i through a linear projection (defined by a weight matrix W) to obtain the individual's embedding $\mathbf{e}_{ind}^i = W[\mathbf{e}_{self}^i; \mathbf{e}_{partner}^i]$. Our intuition is that with information about both p_i themselves, and of p_i 's partners from p_i 's point-of-view, \mathbf{e}_{ind}^i now contains the information required to predict p_i 's future behavior.

Encoding Future Window Offset. As we've discussed at the start of this section, a single \mathbf{t}_{obs} might have multiple associated \mathbf{t}_{fut} windows at different offsets. Our intuition is that training a sequence decoder to decode the same \mathbf{e}_{ind}^i into multiple sequences (corresponding to the multiple \mathbf{t}_{fut}) in the absence of any timing information might cause an averaging effect in either the decoder or the information encoded in \mathbf{e}_{ind}^i . One way around this would be to start decoding one timestep following the end of \mathbf{t}_{obs} and discard the predictions in the gap between \mathbf{t}_{obs} and \mathbf{t}_{fut} . However, if decoding is done auto-regressively this might lead to cascading errors over the gap. Instead, we address this one-to-many issue by injecting the offset information into \mathbf{e}_{ind}^i so that the decoder receives a unique encoded representation for every \mathbf{t}_{fut} to decode over. We do this by repurposing the idea of sinusoidal positional encodings [61] to encode offsets rather than relative positions in sequences. For a given \mathbf{t}_{obs} and \mathbf{t}_{fut} , and d_e -dimensional \mathbf{e}_{ind}^i we define the offset as $\Delta t = f1 - oT$, and the corresponding offset encoding $OE_{\Delta t}$ as

$$OE_{(\Delta t, 2m)} = \sin(\Delta t / 10000^{2m/d_e}), \quad OE_{(\Delta t, 2m+1)} = \cos(\Delta t / 10000^{2m/d_e}). \quad (7a, b)$$

Here m refers to the dimension index in the encoding. We finally compute the representation \mathbf{e}^i for Eqs. 4 and 5 as

$$\mathbf{e}^i = \mathbf{e}_{ind}^i + OE_{\Delta t}. \quad (8)$$

Auxiliary Loss Functions. We incorporate a geometric loss function that improves performance in pose regression tasks. For p_i at time t , given the ground truth $\mathbf{b}_t^i = [\mathbf{q}; \mathbf{l}; s]$, and the predicted mean $\hat{\mathbf{b}}_t^i = [\hat{\mathbf{q}}; \hat{\mathbf{l}}; \hat{s}]$, we denote the tuple $(\mathbf{b}_t^i, \hat{\mathbf{b}}_t^i)$ as B_t^i . We then have the location loss in Euclidean space $\mathcal{L}_l(B_t^i) = \|\mathbf{l} - \hat{\mathbf{l}}\|$, and we can regress the quaternion values using

$$\mathcal{L}_q(B_t^i) = \left\| \mathbf{q} - \frac{\hat{\mathbf{q}}}{\|\hat{\mathbf{q}}\|} \right\|. \quad (9)$$

Kendall and Cipolla [60] show how these losses can be combined using the homoscedastic uncertainties in position and orientation, $\hat{\sigma}_l^2$ and $\hat{\sigma}_q^2$:

$$\mathcal{L}_\sigma(B_t^i) = \mathcal{L}_l(B_t^i) \exp(-\hat{s}_l) + \hat{s}_l + \mathcal{L}_q(B_t^i) \exp(-\hat{s}_q) + \hat{s}_q, \quad (10)$$

where $\hat{s} := \log \hat{\sigma}^2$. Using the binary cross-entropy loss for speaking status $\mathcal{L}_s(B_t^i)$, we have the overall auxiliary loss over $t \in \mathbf{t}_{fut}$:

$$\mathcal{L}_{aux}(\mathbf{Y}, \hat{\mathbf{Y}}) = \sum_i \sum_t \mathcal{L}_\sigma(B_t^i) + \mathcal{L}_s(B_t^i). \quad (11)$$

The parameters of the SP and ASP are trained² by maximizing the ELBO in Eq. 3 and minimizing this auxiliary loss function for each of our sequence decoders.

²Code, processed data, pre-trained models, and test batches for reproduction are available at <https://github.com/chiragraman/social-processes>

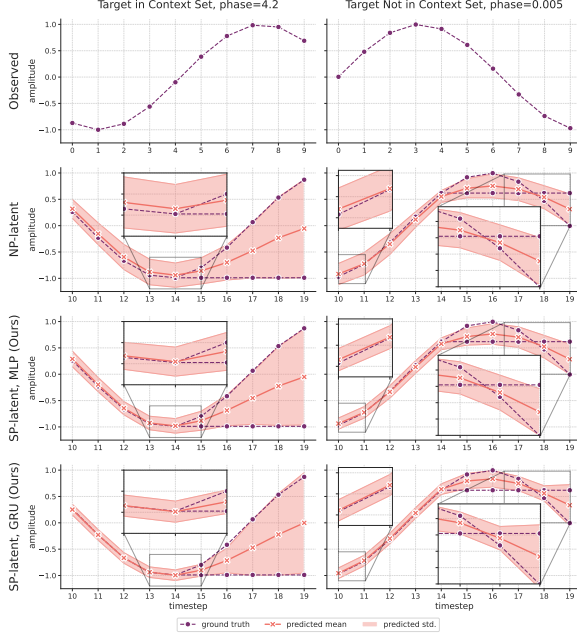


Figure 3: Ground truths and model predictions for the toy task simulating the forecasting of glancing behavior.

6 Experiments and Results

6.1 Models and Baselines

Our modeling assumption is that the underlying stochastic process generating the behaviors does not evolve over time. Stated differently, we assume that the individual factors determining how participants coordinate behaviors—age, cultural background, personality variables [24, Chap. 1; 1, p. 237]—are likely to remain the same over the short duration of a single interaction. This is in contrast to a related line of work that deals with *meta-transfer learning*, where the stochastic process itself changes over time [62–65]. We therefore compare against the NP and ANP family which share our model assumptions and meta-learning attributes. Note that in contrast to our methods, these baselines have direct access to the future sequences in the context, and therefore constitute a strong baseline. We consider two variants: *-latent* denoting only the latent path; and *-latent+det*, containing both deterministic and stochastic paths. We further consider two attention mechanisms for the cross-attention module: *-dot* with dot attention, and *-multihead* with wide multi-head attention [58]. We operationalize the original definitions of the baseline models to sequences by collapsing the timestep and feature dimensions. While the ANP-RNN model [66] shares our model assumptions, it is defined for a task analogous to SSP for concurrent car locations, and cannot be operationalized to forecasting in any simple way (see Section 3 discussing the distinction). We experiment with two choices of architectures for the sequence encoders and decoders in our proposed models: multi-layer perceptrons (MLP), and Gated Recurrent Units (GRU). Implementation and training details for our experiments can be found in Appendix C.

6.2 Evaluation on Synthesized Behavior: Forecasting Glancing Behavior

With limited behavioral data availability, a common practice in the domain is to train and evaluate methods on synthesized behavior dynamics [31, 67]. In keeping with this practice, we construct a synthesized dataset simulating two glancing behaviors in social settings [21]. We use a 1D sinusoid to represent horizontal head rotation over 20 timesteps. The sweeping *Type I* glance is represented by a pristine sinusoid, while the gaze fixating *Type III* glance is denoted by clipping the amplitude for the last six timesteps. The task is to forecast the signal over the last 10 timesteps (t_{fut}) by observing the first 10 (t_{obs}). Consequently, the first half of t_{fut} is certain, while uncertainty over the last half results from every observed sinusoid having two ground-truths. It is impossible to infer from an observed sequence alone if the head rotation will stop partway through the future. We describe

Table 1: Mean (Std.) Negative Log-Likelihood (NLL) on the Haggling Test Sets. The reported mean and std. are over individual sequences in the test sets. Lower is better. The superscript * indicates best NLL within family, boldface best overall.

	Context	
	Random	Fixed-Initial
Baselines		
NP-latent	38.34 (19.1)	37.64 (18.1)
NP-latent+det	40.41 (23.9)	40.15 (23.0)
ANP-dot	35.66* (20.8)	38.06* (20.6)
ANP-multihead	40.60 (19.2)	41.11 (19.2)
Ours (MLP)		
SP-latent	−74.06 (6.0)	−74.19 (5.9)
SP-latent+det	−77.49 (7.8)	−76.90 (8.4)
ASP-dot	−76.33 (6.5)	−75.15 (6.5)
ASP-multihead	−83.77* (10.3)	−83.43* (9.7)
Ours (GRU)		
SP-latent	−4.23 (27.4)	−3.72 (30.7)
SP-latent+det	−17.38* (50.5)	−16.08* (52.2)
ASP-dot	19.91 (46.7)	31.39 (77.0)
ASP-multihead	−7.11 (26.9)	−0.51 (28.8)

additional data setup, model details, and quantitative results for this setting in Appendices A.1, C and D.1, respectively. Figure 3 illustrates the ground truths, predicted means and std. deviations for a sequence within and outside the context set. We observe that all models estimate the mean reasonably well, although our proposed SP models learn a slightly better fit. More crucially, the SP models—especially the SP-GRU—learn much better uncertainty estimates over the certain and uncertain parts of the future compared to the NP baseline.

6.3 Real-World Behavior: The Haggling Dataset

We also evaluate our models on real-world behavior data, using the Haggling dataset of triadic interactions [32]. Participants are engaged in an unscripted game where two sellers compete to sell a fictional product to a buyer who has to choose between the two. We use the same split of 79 training sets (groups) and 28 test sets used by Joo et al. [32]. In our experiments we consider the following social cues: *head pose* described by the 3D location of the nose keypoint and a face normal; *body pose* described by the location of the mid-point of the shoulders and a body normal; and binary *speaking status*. Apart from being the most commonly considered cues in computational analyses of such conversations [68–70], pose and turn taking are found to be crucial in the sustaining of conversation [1, 12, 18]. We specify the dataset preprocessing details in Appendix D.2.

6.4 Evaluation

Context Regimes. We evaluate all models on two context regimes: *random*, and *fixed-initial*. The *random* regime follows the standard NP setting that the models are trained in. Context samples (sequence-pairs) are selected as a random subset of target samples, so the model is exposed to behaviors from any phase of the interaction lifecycle. Here we ensure that batches contain unique t_{obs} to prevent any single observed sequence from dominating the aggregation of representations over the context split. At evaluation, we take 50% of the batch as context. In the *fixed-initial* context regime, we investigate how the model can generalize knowledge of group specific characteristics from observing the initial dynamics of an interaction where certain gestures and patterns are more distinctive [1, Chap. 6]. This matches what a social agent might face in a real-world scenario. Here we treat the first 20% of the entire interaction as context, treating sequences from the rest as target.

Evaluation Metrics. We report the negative log-likelihood (NLL) $-\log p(\mathbf{Y}|\mathbf{X}, C)$ in Table 1 (computed by summing over feature dimensions and people, and averaging over timesteps). Beyond the NLL, we also report the error in the predicted means over test sequences in Table 2: mean-squared error (MSE) for the head and body keypoint locations; mean absolute error (MAE) in orientation in degrees; and speaking status accuracy. Note that while the ground truth orientation normals are constrained in the horizontal plane, we don’t constrain our predicted quaternions. We therefore report the absolute error in rotation in 3D. The reported mean and std. deviation of all metrics are over sequences in the test sets. We further report the metrics for every timestep over t_{fut} in Appendix A.2, and qualitative visualizations of the forecasts in Appendix B.

6.5 Ablations

Encoding Partner Behavior. Modeling the interaction from the perspective of each individual is a central idea in our approach. We investigate the influence of encoding partner behavior into individual representations r_{ind}^i on the performance. We train the SP-latent+det GRU variant in two configurations: *no-pool*, where we do not encode any partner behavior; and *pool-oT* where we pool over partner representations only at the last timestep (similar to [44]). We choose the SP-GRU model since it achieves the best trade-off between minimizing NLL and forecasting cues consistent with human behavior. Both configurations lead to worse NLL and location errors (Appendix A.3).

Deterministic Decoding and Social Encoder Sharing. Error gradients can flow back into our sequence encoders through two paths: from the final stochastic sequence decoder, as well as the deterministic decoders on the latent and deterministic paths. We investigate the effect of the deterministic decoders by training the SP-latent+det GRU model without them. We also investigate sharing a single social encoder between the Process Encoder and Process Decoder in Figure 2. We find that removing the decoders only improves log-likelihood if the encoders are shared, and at the cost of head orientation errors (Appendix A.3).

Table 2: Mean (Std.) Errors in Predicted Means over Sequences in the Hagglng Test Sets. Lower is better for all metrics except for speaking status accuracy. * indicates best measure within family, boldface best overall.

	Random Context					Fixed-Initial Context				
	Head Loc. MSE (cm)	Body Loc. MSE (cm)	Head Ori. MAE (°)	Body Ori. MAE (°)	Speaking Accuracy	Head Loc. MSE (cm)	Body Loc. MSE (cm)	Head Ori. MAE (°)	Body Ori. MAE (°)	Speaking Accuracy
Baselines										
NP-latent	14.21 (6.5)	15.06 (6.1)	16.29 (13.8)	12.82 (13.7)	0.787 (0.23)	13.85 (6.1)	14.71 (5.7)	16.22 (14.1)	12.69* (13.9)	0.774* (0.24)
NP-latent+det	15.01 (7.3)	15.97 (7.2)	17.45 (18.3)	14.65 (20.0)	0.715 (0.24)	15.01 (7.5)	15.95 (7.5)	17.26 (15.9)	14.68 (18.7)	0.701 (0.24)
ANP-dot	11.86* (5.4)	12.22* (5.5)	15.44* (13.3)	12.56* (18.0)	0.806* (0.23)	12.83* (5.9)	13.26* (6.0)	16.19* (13.7)	13.56 (17.8)	0.717 (0.23)
ANP-multihead	16.36 (7.4)	17.17 (7.2)	19.41 (20.4)	16.02 (22.1)	0.692 (0.21)	16.68 (7.9)	17.43 (7.7)	19.78 (21.2)	15.57 (20.3)	0.682 (0.21)
Ours (MLP)										
SP-latent	25.58 (10.1)	26.57* (9.0)	91.07 (23.9)	97.09 (22.5)	0.638 (0.08)	25.27 (10.0)	26.33* (8.9)	91.14 (23.8)	97.09 (22.5)	0.640 (0.09)
SP-latent+det	31.99 (8.2)	36.33 (7.3)	91.08 (23.9)	91.36 (23.9)	0.629 (0.18)	32.93 (9.4)	37.16 (8.5)	91.15 (23.9)	91.36 (23.9)	0.633 (0.18)
ASP-dot	27.16 (7.7)	31.19 (7.1)	90.88 (23.9)	91.43 (23.8)	0.704 (0.19)	27.94 (7.8)	31.83 (7.1)	90.93 (23.9)	91.43 (23.8)	0.628 (0.20)
ASP-multihead	23.88* (7.8)	27.13 (7.7)	90.50* (23.9)	91.04* (24.1)	0.792* (0.24)	24.07* (8.1)	27.35 (8.3)	90.53* (23.9)	91.07* (24.1)	0.770* (0.25)
Ours (GRU)										
SP-latent	17.18 (6.5)	17.41 (6.2)	17.76* (15.8)	14.78* (20.7)	0.713 (0.23)	16.66 (6.2)	17.17 (6.0)	17.67* (16.0)	14.64* (20.3)	0.705 (0.23)
SP-latent+det	15.84 (5.5)	17.76 (7.5)	20.65 (19.9)	21.73 (29.5)	0.671 (0.22)	16.53* (6.0)	18.20 (8.0)	20.74 (19.5)	21.31 (28.9)	0.674 (0.22)
ASP-dot	22.49 (8.7)	22.64 (11.1)	17.99 (12.8)	15.58 (19.6)	0.722 (0.25)	23.66 (8.7)	24.50 (11.7)	19.22 (14.8)	16.82 (19.4)	0.620 (0.27)
ASP-multihead	15.18* (6.7)	15.01* (6.0)	24.26 (21.3)	35.06 (38.5)	0.778* (0.23)	16.84 (6.9)	16.80* (6.3)	25.37 (21.3)	35.44 (38.0)	0.725* (0.23)

7 Discussion and Conclusion

What qualifies as the best performing model for SCF? Our SP-GRU learns the best fit for synthesized behavior. On the commonly used metric of NLL [19, 58, 62], our SP-MLP models perform the best for real-world data. However, they fare the worst at estimating the mean. On the other hand, the SP-GRU models estimate a better likelihood than the NP baselines with comparable errors in mean forecast. While the NP baselines attain the lowest errors in predicted means, they also achieve the worst NLL. From the qualitative visualizations and ablations, it seems that the models minimize NLL at the cost of orientation errors; in the case of SP-MLP seemingly by predicting the majority orientation of the two sellers who face the same direction. Also, the NP models forecast largely static futures. In contrast, while being more dynamic, the SP-GRU forecasts also contain some smoothing.

Our synthesized glancing behavior is grounded in social literature, and matches the head pose features in the real-world data (horizontal orientation). Why do we see a large discrepancy in qualitative forecasts? One crucial distinction between the synthetic and real data is the subtlety and sparsity of motion. Our synthesized data makes the common implicit assumption that head pose is a proxy for gaze [31, 67, 68, 70–72]. In real-world data, attention shifts through changes in gaze are not always accompanied by similar head rotations [73, Fig. 5], and gaze is harder to record non-invasively in-the-wild with reasonable accuracy. The consequence of this approximation is exacerbated in the triadic Hagglng setting where people are arranged roughly in a triangle and within each other’s field of vision, making head movements even more subtle. In natural settings, groups occupy varied formations such as *side-by-side*, or *L-arrangement* [60, p. 213]. Here the more accentuated pose changes could aid in anticipating behavior. From this perspective, the combination of limited data and our simplifying assumption of a single group in a scene is a primary limitation of this work. The only publicly available dataset meeting our assumptions is the Hagglng dataset, where all interactions follow similar patterns. As targeted development of techniques for recording such datasets in-the-wild gain momentum [74], evaluating these models in the different interaction settings would yield increased insight. Nevertheless, our aim in evaluating on synthesized as well as real-world data was to highlight the influence that such common implicit assumptions can have on performance when applying methods. As an aside, we believe that this subtlety and sparsity of motion is also an important distinction between forecasting in focused and unfocused interactions. While the same techniques can be applied in both scenarios, pedestrian location is a perpetually changing data stream.

The broader goal of this paper is to take a step towards bridging a gap we perceive between research domains; on one hand, we notice that there is a growing trend of applying deep learning techniques in the small data regime that is social behavior data [30, 75]. Without citing specific works as negative exemplars, this is occasionally accompanied by surface treatment of social science literature. On the other hand, in our conversations we have also perceived a preemptive resistance to deep learning methods precisely due to limited data. We believe that our work here—specifically our conceptualization of conversations groups as meta-learning *tasks* grounded in extensive considerations from social literature; our approach of learning extractable task-agnostic representations of predictive behavior; and the distinction between real-world and synthesized dynamics commonly used for evaluation—is of value in stimulating a broader community discussion about the considerations when applying machine learning approaches within the domain of free-standing social conversations.

Acknowledgments and Disclosure of Funding

This research was partially funded by the Netherlands Organization for Scientific Research (NWO) under the MINGLE project number 639.022.606. Chirag would like to thank Amelia Villegas-Morcillo for her input and the numerous discussions, and Tiffany Matej Hrkalic and Bernd Dudzik for their feedback on the manuscript.

References

- [1] Adam Kendon. *Conducting Interaction: Patterns of Behavior in Focused Encounters*. Number 7 in Studies in Interactional Sociolinguistics. Cambridge University Press, Cambridge ; New York, 1990. ISBN 978-0-521-38036-2 978-0-521-38938-9.
- [2] Alessandro Vinciarelli, Maja Pantic, and Hervé Bourlard. Social signal processing: Survey of an emerging domain.
- [3] Dan Bohus and Eric Horvitz. Models for multiparty engagement in open-world dialog. In *Proceedings of the SIGDIAL 2009 Conference on The 10th Annual Meeting of the Special Interest Group on Discourse and Dialogue - SIGDIAL '09*, pages 225–234, London, United Kingdom, 2009. Association for Computational Linguistics. ISBN 978-1-932432-64-0. doi: 10.3115/1708376.1708409.
- [4] Ryo Ishii, Shiro Kumano, and Kazuhiro Otsuka. Prediction of Next-Utterance Timing using Head Movement in Multi-Party Meetings. In *Proceedings of the 5th International Conference on Human Agent Interaction, HAI '17*, pages 181–187, New York, NY, USA, October 2017. Association for Computing Machinery. ISBN 978-1-4503-5113-3. doi: 10.1145/3125739.3125765.
- [5] Anne Keitel and Moritz M Daum. The use of intonation for turn anticipation in observed conversations without visual signals as source of information. *Frontiers in psychology*, 6:108, 2015.
- [6] Simon Garrod and Martin J Pickering. The use of content and timing to predict turn transitions. *Frontiers in psychology*, 6:751, 2015.
- [7] Amélie Rochet-Capellan and Susanne Fuchs. Take a breath and take the turn: how breathing meets turns in spontaneous dialogue. *Philosophical Transactions of the Royal Society B: Biological Sciences*, 369(1658): 20130399, 2014.
- [8] M. Wlodarczyk and M. Heldner. Respiratory turn-taking cues. In *INTERSPEECH*, 2016.
- [9] Dan Bohus and Eric Horvitz. Managing Human-Robot Engagement with Forecasts and. . . um. . . Hesitations. page 8.
- [10] Cynthia C. S. Liem, Markus Langer, Andrew Demetriou, Annemarie M. F. Hiemstra, Achmadnoer Sukma Wicaksana, Marise Ph. Born, and Cornelius J. König. Psychology Meets Machine Learning: Interdisciplinary Perspectives on Algorithmic Job Candidate Screening. In *Explainable and Interpretable Models in Computer Vision and Machine Learning*, 2018. ISBN 978-3-319-98130-7 978-3-319-98131-4.
- [11] Erlend Nilsen, Diana Bowler, and John Linnell. Exploratory and confirmatory research in the open science era. *Journal of Applied Ecology*, 57, February 2020. doi: 10.1111/1365-2664.13571.
- [12] Starkey Duncan. Some signals and rules for taking speaking turns in conversations. *Journal of Personality and Social Psychology*, 23(2):283–292, 1972. ISSN 1939-1315(Electronic),0022-3514(Print). doi: 10.1037/h0033031.
- [13] Akko Kalma. Gazing in triads: A powerful signal in floor apportionment. *British Journal of Social Psychology*, 31(1):21–39, March 1992.
- [14] Sanjay Bilakhia, Stavros Petridis, and Maja Pantic. Audiovisual Detection of Behavioural Mimicry. In *2013 Humaine Association Conference on Affective Computing and Intelligent Interaction*, pages 123–128, Geneva, Switzerland, September 2013. IEEE. ISBN 978-0-7695-5048-0. doi: 10.1109/ACII.2013.27.
- [15] Felix van Doorn. Rituals of Leaving: Predictive Modelling of Leaving Behaviour in Conversation. *Master of Science Thesis, Delft University of Technology*, 2018.
- [16] Laura Cabrera-Quiros, Andrew Demetriou, Ekin Gedik, Leander van der Meij, and Hayley Hung. The matchnmingle dataset: a novel multi-sensor resource for the analysis of social interactions and group dynamics in-the-wild during free-standing conversations and speed dates. *IEEE Transactions on Affective Computing*, 2018.
- [17] Nalini Ambady, Frank J Bernieri, and Jennifer A Richeson. Toward a histology of social behavior: Judgmental accuracy from thin slices of the behavioral stream. In *Advances in experimental social psychology*, volume 32, pages 201–271. Elsevier, 2000.
- [18] Alessandro Vinciarelli, H Salamin, and M Pantic. Social Signal Processing: Understanding social interactions through nonverbal behavior analysis (PDF). *2009 IEEE Conference on Computer Vision and Pattern Recognition, CVPR 2009*, June 2009. doi: 10.1109/CVPRW.2009.5204290.

- [19] Marta Garnelo, Jonathan Schwarz, Dan Rosenbaum, Fabio Viola, Danilo J. Rezende, S. M. Ali Eslami, and Yee Whye Teh. Neural Processes. *arXiv:1807.01622 [cs, stat]*, 2018.
- [20] Mattias Heldner and Jens Edlund. Pauses, gaps and overlaps in conversations. *Journal of Phonetics*, 38(4): 555–568, October 2010. ISSN 0095-4470. doi: 10.1016/j.wocn.2010.08.002.
- [21] Monica M. Moore. Nonverbal courtship patterns in women: Context and consequences. *Ethology and Sociobiology*, 6(4):237–247, January 1985. ISSN 0162-3095. doi: 10.1016/0162-3095(85)90016-0.
- [22] Stephen C. Levinson and Francisco Torreira. Timing in turn-taking and its implications for processing models of language. *Frontiers in Psychology*, 6, June 2015. ISSN 1664-1078. doi: 10.3389/fpsyg.2015.00731.
- [23] Erving Goffman. *Behavior in Public Places: Notes on the Social Organization of Gatherings*. The Free Press, 1. paperback ed., 24. printing edition. ISBN 978-0-02-911940-2.
- [24] Nina-Jo Moore, Hickson Mark III, and W Don. Stacks. Nonverbal communication: Studies and applications. 2013.
- [25] Harvey Sacks, Emanuel A. Schegloff, and Gail Jefferson. A Simplest Systematics for the Organization of Turn-Taking for Conversation. 50(4):40, 1974.
- [26] Charles Goodwin. *Conversational Organization: Interaction Between Speakers and Hearers*. January 1981.
- [27] Carole Edelsky. Who’s Got the Floor? *Language in Society*, 10(3):383–421, 1981. ISSN 0047-4045.
- [28] Allan Wang and Aaron Steinfeld. Group Split and Merge Prediction With 3D Convolutional Networks. *IEEE Robotics and Automation Letters*, 5(2):1923–1930, April 2020. ISSN 2377-3766. doi: 10.1109/LRA.2020.2969947.
- [29] Massimo Mastrangeli, Martin Schmidt, and Lucas Lacasa. The roundtable: An abstract model of conversation dynamics. *arXiv:1010.2943 [physics]*, October 2010.
- [30] Louis Airale, Dominique Vaufreydaz, and Xavier Alameda-Pineda. SocialInteractionGAN: Multi-person Interaction Sequence Generation. *arXiv:2103.05916 [cs, stat]*, March 2021.
- [31] Navyata Sanghvi, Ryo Yonetani, and Kris Kitani. Mgpi: A computational model of multiagent group perception and interaction. *arXiv preprint arXiv:1903.01537*, 2019.
- [32] Hanbyul Joo, Tomas Simon, Mina Cikara, and Yaser Sheikh. Towards Social Artificial Intelligence: Nonverbal Social Signal Prediction in a Triadic Interaction. In *2019 IEEE/CVF Conference on Computer Vision and Pattern Recognition (CVPR)*, pages 10865–10875, Long Beach, CA, USA, June 2019. IEEE. ISBN 978-1-72813-293-8. doi: 10.1109/CVPR.2019.01113.
- [33] Emilie Delaherche, Mohamed Chetouani, Ammar Mahdhaoui, Catherine Saint-Georges, Sylvie Viaux, and David Cohen. Interpersonal Synchrony: A Survey of Evaluation Methods across Disciplines. *IEEE Transactions on Affective Computing*, 3(3):349–365, July 2012. ISSN 1949-3045. doi: 10.1109/T-AFFC.2012.12.
- [34] Dirk Helbing and Peter Molnar. Social Force Model for Pedestrian Dynamics. *Physical Review E*, 51(5): 4282–4286, May 1995. ISSN 1063-651X, 1095-3787. doi: 10.1103/PhysRevE.51.4282.
- [35] Jarosław Wąs, Bartłomiej Gudowski, and Paweł J. Matuszyk. Social Distances Model of Pedestrian Dynamics. In *Cellular Automata*, volume 4173, pages 492–501. Springer Berlin Heidelberg, Berlin, Heidelberg, 2006. ISBN 978-3-540-40929-8 978-3-540-40932-8. doi: 10.1007/11861201_57.
- [36] Gianluca Antonini, Michel Bierlaire, and Mats Weber. Discrete Choice Models for Pedestrian Walking Behavior. *Transportation Research Part B: Methodological*, 40:667–687, September 2006. doi: 10.1016/j.trb.2005.09.006.
- [37] Adrien Treuille, Seth Cooper, and Zoran Popović. Continuum crowds. *ACM Transactions on Graphics / SIGGRAPH 2006*, 25(3):1160–1168, July 2006.
- [38] Alexandre Robicquet, Amir Sadeghian, Alexandre Alahi, and Silvio Savarese. Learning Social Etiquette: Human Trajectory Understanding In Crowded Scenes. In *Computer Vision – ECCV 2016*, volume 9912, pages 549–565. Springer International Publishing, Cham, 2016. ISBN 978-3-319-46483-1 978-3-319-46484-8. doi: 10.1007/978-3-319-46484-8_33.
- [39] J. M. Wang, D. J. Fleet, and A. Hertzmann. Gaussian Process Dynamical Models for Human Motion. *IEEE Transactions on Pattern Analysis and Machine Intelligence*, 30(2):283–298, February 2008. ISSN 1939-3539. doi: 10.1109/TPAMI.2007.1167.
- [40] Christopher Tay and Christian Laugier. Modelling Smooth Paths Using Gaussian Processes. In *Proc. of the Int. Conf. on Field and Service Robotics*, 2007.
- [41] Andrew Patterson, Arun Lakshmanan, and Naira Hovakimyan. Intent-Aware Probabilistic Trajectory Estimation for Collision Prediction with Uncertainty Quantification. *arXiv:1904.02765 [cs, math]*, April 2019.

- [42] Alexandre Alahi, Kratarth Goel, Vignesh Ramanathan, Alexandre Robicquet, Li Fei-Fei, and Silvio Savarese. Social LSTM: Human Trajectory Prediction in Crowded Spaces. In *2016 IEEE Conference on Computer Vision and Pattern Recognition (CVPR)*, pages 961–971, Las Vegas, NV, USA, June 2016. IEEE. ISBN 978-1-4673-8851-1. doi: 10.1109/CVPR.2016.110.
- [43] Pu Zhang, Wanli Ouyang, Pengfei Zhang, Jianru Xue, and Nanning Zheng. SR-LSTM: State Refinement for LSTM towards Pedestrian Trajectory Prediction. *arXiv:1903.02793 [cs]*, March 2019.
- [44] Agrim Gupta, Justin Johnson, Li Fei-Fei, Silvio Savarese, and Alexandre Alahi. Social GAN: Socially Acceptable Trajectories with Generative Adversarial Networks. *arXiv:1803.10892 [cs]*, March 2018.
- [45] Yingfan Huang, Huikun Bi, Zhaoxin Li, Tianlu Mao, and Zhaoqi Wang. STGAT: Modeling Spatial-Temporal Interactions for Human Trajectory Prediction. In *2019 IEEE/CVF International Conference on Computer Vision (ICCV)*, pages 6271–6280, Seoul, Korea (South), October 2019. IEEE. ISBN 978-1-72814-803-8. doi: 10.1109/ICCV.2019.00637.
- [46] Abdullah Mohamed, Kun Qian, Mohamed Elhoseiny, and Christian Claudel. Social-STGCNN: A Social Spatio-Temporal Graph Convolutional Neural Network for Human Trajectory Prediction. *arXiv:2002.11927 [cs]*, February 2020.
- [47] MarcAurelio Ranzato, Arthur Szlam, Joan Bruna, Michael Mathieu, Ronan Collobert, and Sumit Chopra. Video (language) modeling: A baseline for generative models of natural videos. *arXiv:1412.6604 [cs]*, December 2014.
- [48] Jacob Walker, Kenneth Marino, Abhinav Gupta, and Martial Hebert. The Pose Knows: Video Forecasting by Generating Pose Futures. *arXiv:1705.00053 [cs]*, April 2017.
- [49] Jacob Walker, Abhinav Gupta, and Martial Hebert. Dense Optical Flow Prediction from a Static Image. In *2015 IEEE International Conference on Computer Vision (ICCV)*, pages 2443–2451, Santiago, Chile, December 2015. IEEE. ISBN 978-1-4673-8391-2. doi: 10.1109/ICCV.2015.281.
- [50] Alexey Dosovitskiy, Philipp Fischer, Eddy Ilg, Philip Hausser, Caner Hazirbas, Vladimir Golkov, Patrick van der Smagt, Daniel Cremers, and Thomas Brox. FlowNet: Learning Optical Flow with Convolutional Networks. In *2015 IEEE International Conference on Computer Vision (ICCV)*, pages 2758–2766, Santiago, December 2015. IEEE. ISBN 978-1-4673-8391-2. doi: 10.1109/ICCV.2015.316.
- [51] Jacob Walker, Abhinav Gupta, and Martial Hebert. Patch to the Future: Unsupervised Visual Prediction. In *2014 IEEE Conference on Computer Vision and Pattern Recognition*, pages 3302–3309, Columbus, OH, USA, June 2014. IEEE. ISBN 978-1-4799-5118-5. doi: 10.1109/CVPR.2014.416.
- [52] Carl Vondrick, Hamed Pirsiavash, and Antonio Torralba. Anticipating Visual Representations from Unlabeled Video. In *2016 IEEE Conference on Computer Vision and Pattern Recognition (CVPR)*, pages 98–106, Las Vegas, NV, USA, June 2016. IEEE. ISBN 978-1-4673-8851-1. doi: 10.1109/CVPR.2016.18.
- [53] Nitish Srivastava, Elman Mansimov, and Ruslan Salakhutdinov. Unsupervised Learning of Video Representations using LSTMs. *arXiv:1502.04681 [cs]*, February 2015.
- [54] Alexey Dosovitskiy and Vladlen Koltun. Learning to Act by Predicting the Future. *arXiv:1611.01779 [cs]*, November 2016.
- [55] Timothy Hospedales, Antreas Antoniou, Paul Micaelli, and Amos Storkey. Meta-Learning in Neural Networks: A Survey. *arXiv:2004.05439 [cs, stat]*, November 2020.
- [56] Ilya Sutskever, Oriol Vinyals, and Quoc V Le. Sequence to Sequence Learning with Neural Networks. In Z. Ghahramani, M. Welling, C. Cortes, N. D. Lawrence, and K. Q. Weinberger, editors, *Advances in Neural Information Processing Systems 27*, pages 3104–3112. Curran Associates, Inc., 2014.
- [57] Kyunghyun Cho, Bart van Merriënboer, Caglar Gulcehre, Dzmitry Bahdanau, Fethi Bougares, Holger Schwenk, and Yoshua Bengio. Learning Phrase Representations using RNN Encoder-Decoder for Statistical Machine Translation. *arXiv:1406.1078 [cs, stat]*, September 2014.
- [58] Hyunjik Kim, Andriy Mnih, Jonathan Schwarz, Marta Garnelo, Ali Eslami, Dan Rosenbaum, Oriol Vinyals, and Yee Whye Teh. Attentive Neural Processes. *arXiv:1901.05761 [cs, stat]*, July 2019.
- [59] Charles R. Qi, Hao Su, Kaichun Mo, and Leonidas J. Guibas. PointNet: Deep Learning on Point Sets for 3D Classification and Segmentation. *arXiv:1612.00593 [cs]*, April 2017.
- [60] Alex Kendall and Roberto Cipolla. Geometric Loss Functions for Camera Pose Regression with Deep Learning. *arXiv:1704.00390 [cs]*, May 2017.
- [61] Ashish Vaswani, Noam Shazeer, Niki Parmar, Jakob Uszkoreit, Llion Jones, Aidan N. Gomez, Lukasz Kaiser, and Illia Polosukhin. Attention Is All You Need. *arXiv:1706.03762 [cs]*, June 2017.
- [62] Gautam Singh, Jaesik Yoon, Youngsung Son, and Sungjin Ahn. Sequential Neural Processes. URL <http://arxiv.org/abs/1906.10264>.
- [63] Jaesik Yoon, Gautam Singh, and Sungjin Ahn. Robustifying Sequential Neural Processes. In *International Conference on Machine Learning*, pages 10861–10870. PMLR, November 2020.

- [64] Timon Willi, Jonathan Masci, Jürgen Schmidhuber, and Christian Osendorfer. Recurrent Neural Processes. *arXiv:1906.05915 [cs, stat]*, November 2019.
- [65] Sumit Kumar. Spatiotemporal Modeling using Recurrent Neural Processes. *Master of Science Thesis, Carnegie Mellon University*, page 43.
- [66] Shenghao Qin, Jiacheng Zhu, Jimmy Qin, Wenshuo Wang, and Ding Zhao. Recurrent Attentive Neural Process for Sequential Data. *arXiv:1910.09323 [cs, stat]*, October 2019.
- [67] Marynel Vazquez, Aaron Steinfeld, and Scott E. Hudson. Maintaining awareness of the focus of attention of a conversation: A robot-centric reinforcement learning approach. In *2016 25th IEEE International Symposium on Robot and Human Interactive Communication (RO-MAN)*, pages 36–43, New York, NY, USA, August 2016. IEEE. ISBN 978-1-5090-3929-6. doi: 10.1109/ROMAN.2016.7745088.
- [68] Xavier Alameda-Pineda, Yan Yan, Elisa Ricci, Oswald Lanz, and Nicu Sebe. Analyzing Free-standing Conversational Groups: A Multimodal Approach. pages 5–14. ACM Press, 2015. ISBN 978-1-4503-3459-4. doi: 10.1145/2733373.2806238.
- [69] Lu Zhang and Hayley Hung. On Social Involvement in Mingling Scenarios: Detecting Associates of F-formations in Still Images. *IEEE Transactions on Affective Computing*, 2018.
- [70] Stephanie Tan, David M. J. Tax, and Hayley Hung. Multimodal Joint Head Orientation Estimation in Interacting Groups via Proxemics and Interaction Dynamics. *Proceedings of the ACM on Interactive, Mobile, Wearable and Ubiquitous Technologies*, 5(1):1–22, March 2021. ISSN 2474-9567. doi: 10.1145/3448122.
- [71] Rutger Rienks, Ronald Poppe, and Mannes Poel. Speaker Prediction based on Head Orientations. page 7.
- [72] M. Farenzena, A. Tavano, L. Bazzani, D. Tosato, G. Paggetti, G. Menegaz, V. Murino, and M. Cristani. Social interactions by visual focus of attention in a three-dimensional environment. *Expert Systems*, 30(2): 115–127, May 2013. ISSN 02664720. doi: 10.1111/j.1468-0394.2012.00622.x.
- [73] S.O. Ba and J.-M. Odobez. Recognizing Visual Focus of Attention From Head Pose in Natural Meetings. *IEEE Transactions on Systems, Man, and Cybernetics, Part B (Cybernetics)*, 39(1):16–33, February 2009. ISSN 1083-4419. doi: 10.1109/TSMCB.2008.927274.
- [74] Chirag Raman, Stephanie Tan, and Hayley Hung. A modular approach for synchronized wireless multimodal multisensor data acquisition in highly dynamic social settings. *arXiv preprint arXiv:2008.03715*, 2020.
- [75] Mason Swofford, John Charles Peruzzi, Nathan Tsoi, Sydney Thompson, Roberto Martín-Martín, Silvio Savarese, and Marynel Vázquez. Improving Social Awareness Through DANTE: A Deep Affinity Network for Clustering Conversational Interactants. *Proceedings of the ACM on Human-Computer Interaction*, 4 (CSCW1):1–23, May 2020. ISSN 2573-0142. doi: 10.1145/3392824.
- [76] Tuan Anh Le, Hyunjik Kim, and Marta Garnelo. Empirical Evaluation of Neural Process Objectives. page 9.
- [77] Diederik P. Kingma and Jimmy Ba. Adam: A Method for Stochastic Optimization. *arXiv:1412.6980 [cs]*, January 2017.
- [78] Adam Paszke, Sam Gross, Francisco Massa, Adam Lerer, James Bradbury, Gregory Chanan, Trevor Killeen, Zeming Lin, Natalia Gimelshein, Luca Antiga, Alban Desmaison, Andreas Kopf, Edward Yang, Zachary DeVito, Martin Raison, Alykhan Tejani, Sasank Chilamkurthy, Benoit Steiner, Lu Fang, Junjie Bai, and Soumith Chintala. Pytorch: An imperative style, high-performance deep learning library. In *Advances in Neural Information Processing Systems 32*, pages 8024–8035. Curran Associates, Inc., 2019.
- [79] WA Falcon et al. Pytorch lightning. *GitHub. Note: <https://github.com/PyTorchLightning/pytorch-lightning>*, 3, 2019.
- [80] Chirag Raman and Hayley Hung. Towards automatic estimation of conversation floors within f-formations. In *2019 8th International Conference on Affective Computing and Intelligent Interaction Workshops and Demos (ACIIW)*, pages 175–181. IEEE, 2019.

A Detailed Results

A.1 Quantitative Results: Forecasting Glancing Behavior

Table 3 depicts the NLL and head orientation error metrics for our experiments on the task of forecasting glancing behavior using synthetic data. All models are evaluated under the *random* context regime and *no-pool* configuration. The sinusoids are interpreted to represent a horizontal head rotation between -90° and 90° . To provide further insight into model performance, in Figure 4 we plot the MAE in predicted and expected mean forecasts averaged over t_{fut} against the phase of the sinusoids in the dataset. We observe that the SP-GRU error plot is smoother with respect to small phase changes, with lower errors overall.

Table 3: Mean (Std.) Metrics on the Synthetic Glancing Behavior Dataset. The metrics are averaged over timesteps; mean and std. are then computed over sequences. Lower is better. Boldface indicates best overall.

	NLL	Head Ori. MAE ($^\circ$)
Baseline		
NP-latent	-0.281 (0.239)	19.631 (7.260)
Ours		
SP-latent (MLP)	-0.361 (0.197)	19.461 (7.049)
SP-latent (GRU)	-0.552 (0.230)	18.55 (7.109)

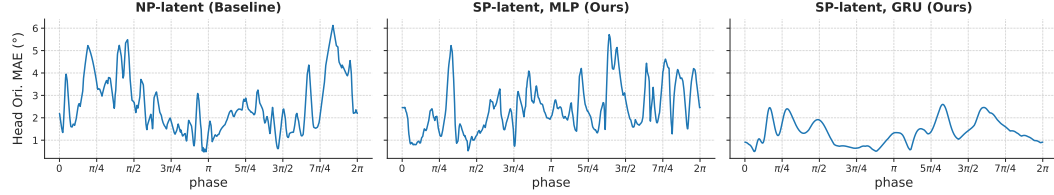


Figure 4: Error in forecast mean and expected mean orientation (average of the two ground-truth futures) for every sequence in the Synthetic Glancing dataset. Each sequence is denoted by the phase of the sinusoid.

A.2 Per Timestep Metrics

In Figure 5 we plot the evaluation metrics per timestep averaged over sequences in the Synthetic Glancing Behavior dataset. In Figure 6 we do the same for sequences in the Haggling Test Sets.

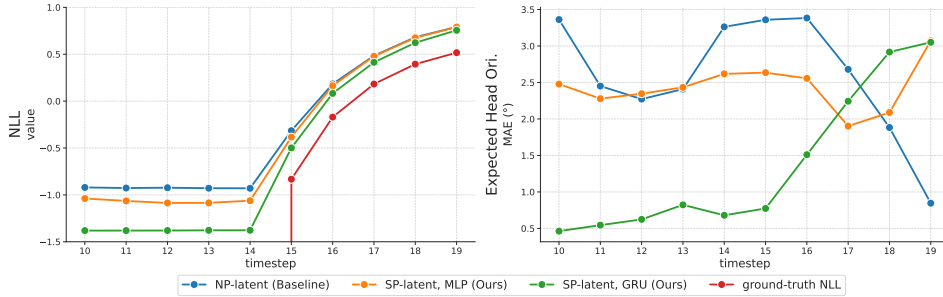


Figure 5: Mean Per Timestep Metrics over the Sequences in the Synthetic Glancing Dataset. NLL is expected to increase over timesteps where ground-truth futures diverge, being $-\infty$ when the future is certain. Head orientation error is computed between the predicted mean and the expected mean (average of the two ground-truth futures). We observe that the SP-GRU model performs best, especially when the future is certain, learning both the best mean and std. over those timesteps.

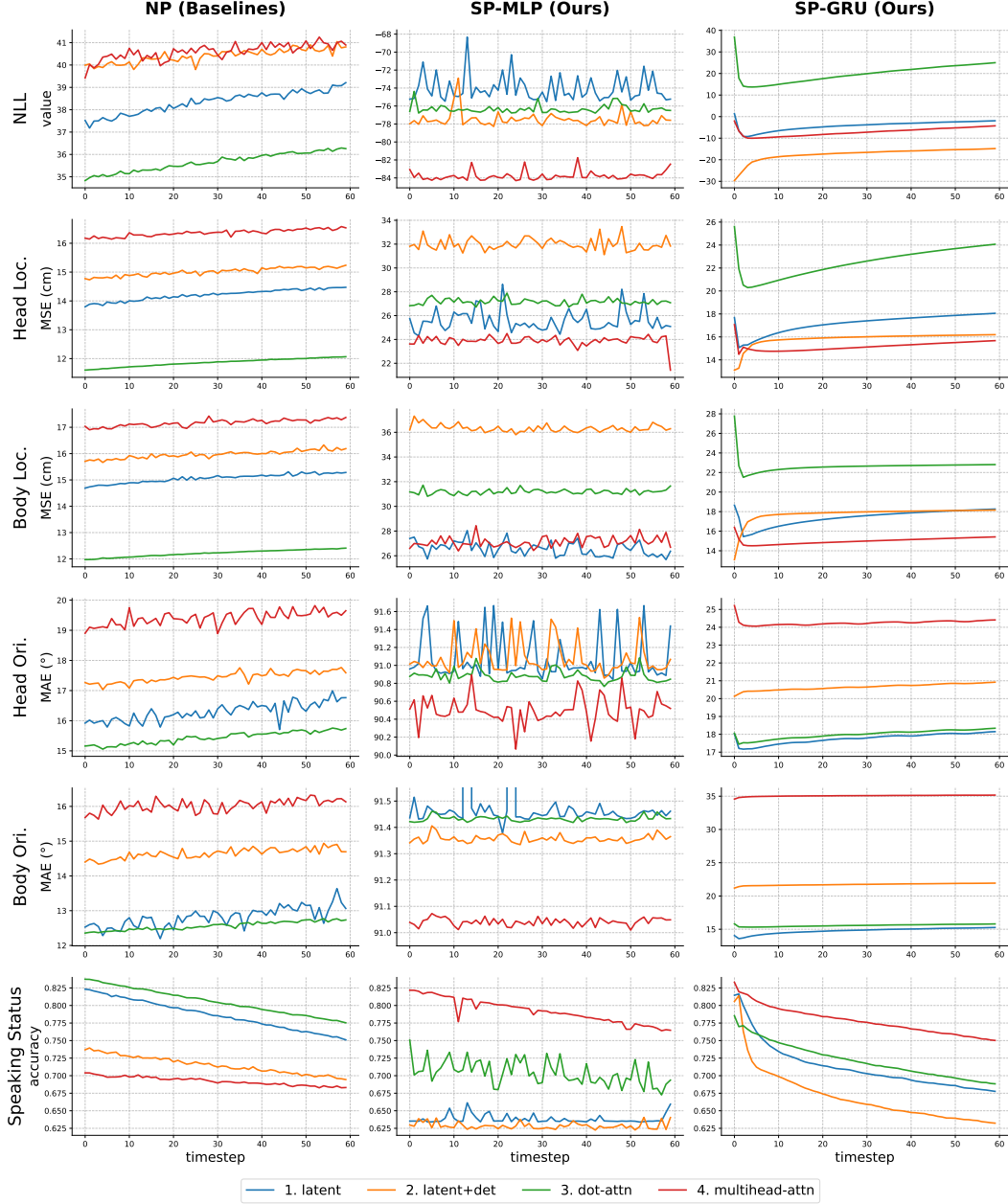


Figure 6: Mean Per Timestep Metrics over the Sequences in the Haggling Test Sets. Note that the y-axes do not share the same scale, except for speaking status accuracy. We observe that the SP-GRU model predicts smooth futures unlike the MLP models. There is a slight trend that the models get worse at forecasting over the duration of t_{fut} .

A.3 Ablations

Table 4: Mean (Std.) NLL for the Ablation Experiments with the SP-latent+det GRU Model. The reported mean and std. are over sequences in the Hagglng Test Sets. Lower is better.

	Context	
	Random	Fixed-Initial
Full Model	-17.38 (50.5)	-16.08 (52.2)
Encoding Partner Behavior		
no-pool	8.02 (75.5)	12.39 (97.5)
pool-oT	-4.67 (26.9)	-4.50 (26.7)
No Deterministic Decoding		
Shared Social Encoders	-30.65 (39.3)	-29.45 (40.4)
Unshared Social Encoders	-3.81 (28.3)	-1.79 (27.3)

Table 5: Mean (Std.) Errors in Predicted Means for the Ablation Experiments with the SP-latent+det GRU Model. The reported mean and std. are over sequences in the Hagglng Test Sets. Lower is better for all except for speaking status accuracy.

	Random Context					Fixed-Initial Context				
	Head Loc. MSE (cm)	Body Loc. MSE (cm)	Head Ori. MAE (°)	Body Ori. MAE (°)	Speaking Accuracy	Head Loc. MSE (cm)	Body Loc. MSE (cm)	Head Ori. MAE (°)	Body Ori. MAE (°)	Speaking Accuracy
Full Model	15.84 (5.5)	17.76 (7.5)	20.65 (19.9)	21.73 (29.5)	0.671 (0.22)	16.53 (6.0)	18.20 (8.0)	20.74 (19.5)	21.31 (28.9)	0.674 (0.22)
Encoding Partner Behavior										
no-pool	18.20 (6.7)	18.05 (7.7)	16.76 (12.8)	14.30 (20.9)	0.690 (0.21)	18.64 (6.7)	18.45 (7.4)	16.85 (12.9)	14.29 (20.5)	0.687 (0.21)
pool-oT	17.42 (6.2)	19.31 (6.3)	23.39 (24.9)	17.68 (26.9)	0.743 (0.21)	17.83 (6.2)	19.23 (6.3)	23.53 (24.3)	17.51 (25.7)	0.735 (0.22)
No Deterministic Decoding										
Shared Social Encoders	15.76 (7.2)	16.34 (6.6)	45.54 (44.6)	21.87 (25.0)	0.644 (0.22)	16.93 (8.1)	17.15 (7.0)	45.49 (44.3)	21.83 (24.7)	0.637 (0.22)
Unshared Social Encoders	17.40 (6.9)	18.33 (6.7)	18.62 (14.7)	14.54 (20.2)	0.704 (0.23)	18.54 (7.9)	19.18 (7.1)	18.68 (14.9)	14.44 (20.0)	0.700 (0.23)

B Qualitative Visualizations

B.1 Glancing Behavior

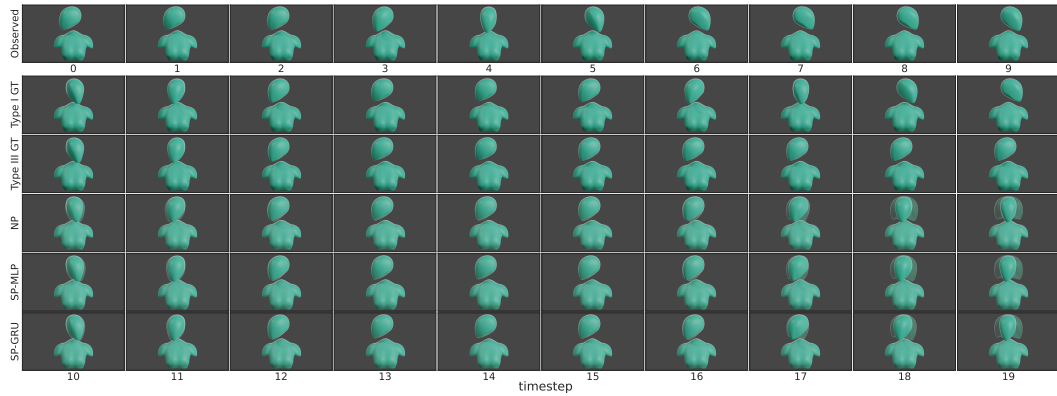


Figure 7: Forecasting Glancing Behavior for a Sequence in the Context Set. We visualize the same sinusoid within the context set as plotted in Figure 3 (phase = 4.2), here interpreted as a horizontal head rotation between -90° and 90° . The bottom three rows depict predictions, with the solid head denoting the mean, and the translucent heads the std. *GT* stands for *Ground-Truth*. The SP models learn better uncertainty estimates, especially over the timesteps where the future is certain (see timestep 11, for instance).

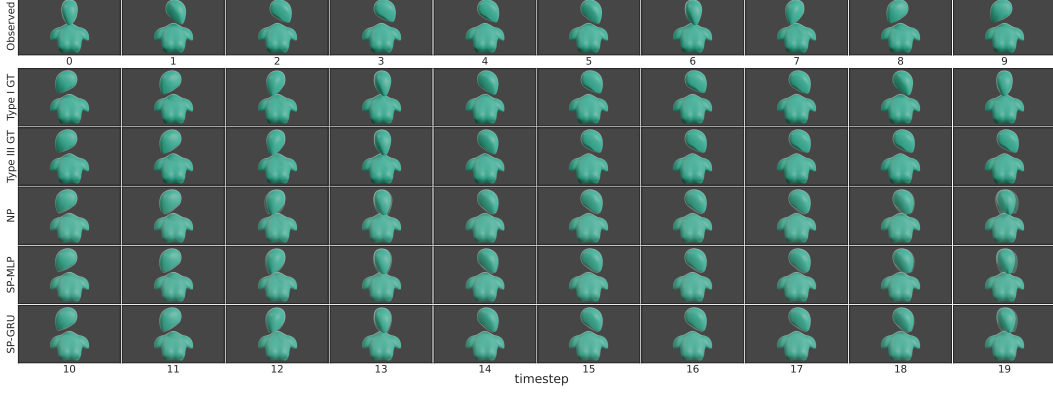


Figure 8: Forecasting Glancing Behavior for a Sequence Not in the Context Set. We visualize the same sinusoid not in the context set as plotted in Figure 3 (phase = 0.005). See the Figure 7 caption for details.

B.2 Hagglng

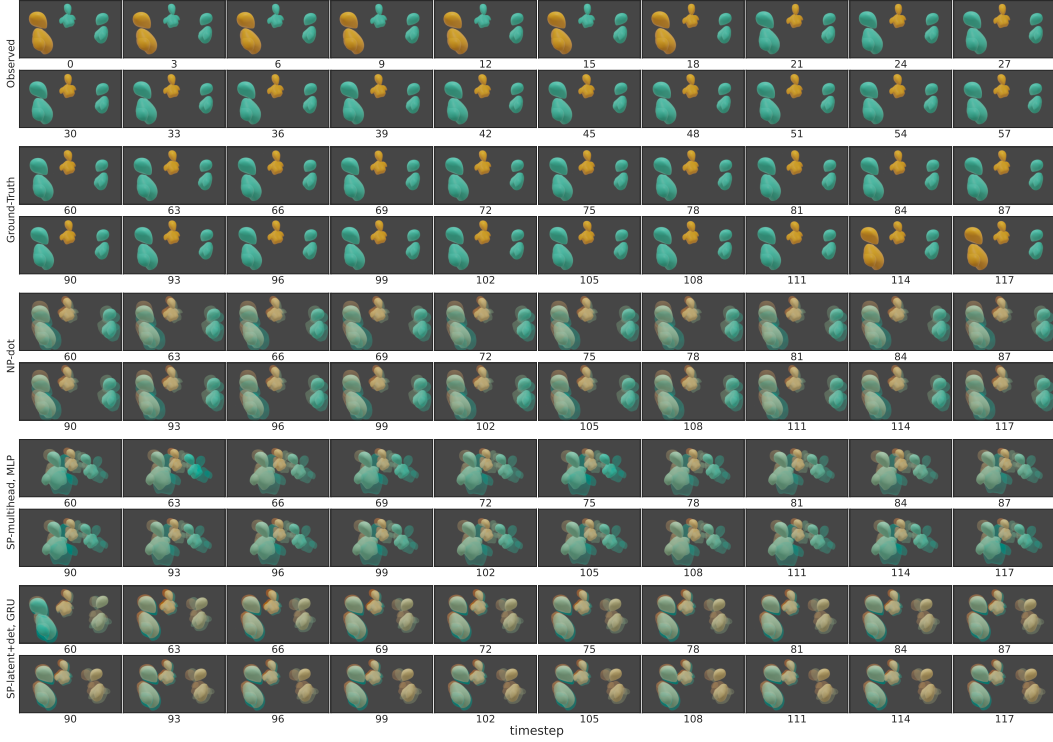


Figure 9: Forecasts for a Sequence from the Hagglng Test Group 170221-b1-group3. Note that these are features from real-world data visualized using 3D models. Speakers are depicted in orange and listeners in green. The predicted speaking status mean is visualized as an interpolated shade between the two colors. The translucent models in the forecasts denote the mean \pm std. pose and speaking status. We observe that the NP forecasts are almost completely static. The SP-GRU forecasts are comparatively dynamic with lower uncertainties overall. The SP-MLP model seems to be learning an overall average orientation, forecasting all participants to be facing in the direction of the two sellers. Note that the pose changes are far more subtle than in the glancing behavior dataset. Interaction videos reveal that the participants significantly rely on gaze changes to direct attention. See Section 7 for a discussion.

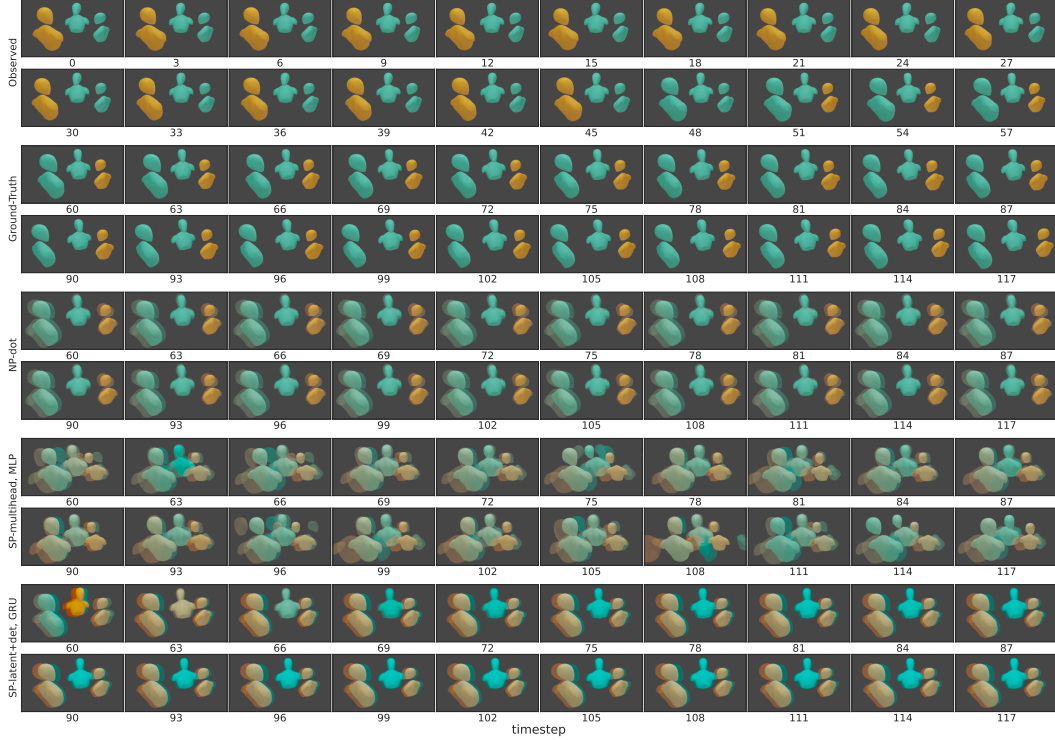


Figure 10: Forecasts for a Sequence from the Hagglng Train Group 170224-a1-group1. We see a similar pattern to the model forecasts as in Figure 9: NP forecasts are static, SP-GRU predicts more dynamic futures, while the SP-MLP forecast average orientations. A turn change has occurred at the end of the observed window. We observe that the SP-GRU model forecasts an interesting continuation to the turn. It anticipates the buyer (middle) to quickly interject the last observed speaking seller, before falling silent and directing attention between the sellers, both of whom it expects to then speak simultaneously. While this is not the ground-truth future in this instance, we believe that the forecast still indicates that the model is capable of learning believable haggling turn dynamics from the overall training data. See the Figure 9 for details on the visualization setup.

C Implementation Details

C.1 Neural Architectures

The data dimension for the experiments on the Hagglng dataset is 15, while that for the toy glancing experiment is 1. Table 6 specifies the network architecture hyperparameters for the Hagglng dataset experiments. For the toy experiment, all the hidden and representation dimensions are fixed at 32.

The goal of our experiments is to evaluate the relative impact of our modeling choices on performance, rather than finding the best possible model for benchmarking. Consequently, we chose a set of architecture hyperparameters such that the simplest *-latent* variants have a comparable number of parameters for cross-family comparison. These hyperparameters were then kept fixed for the variants within each family for fair intra-family comparison. The hyperparameters we chose resulted from light tuning through 5-fold cross-validation and showed improved performance for all models, but improved absolute performance might be obtained through more extensive tuning.

C.2 Training and Evaluation

We construct batches for training by bucketing samples such that all sequences in a batch share the same t_{obs} , and the same t_{fut} length. Note that since the MLP models are operationalized by collapsing the timestep and feature dimensions, the length of t_{obs} and t_{fut} is the same for these models across batches. However, since the recurrent models can handle sequences of different lengths, we allow for forecasting different length futures across batches resulting in a few more training batches. Following the training practices suggested by Le et al. [76], we construct the context set at training as a random

Table 6: Architecture Hyperparameters for the Haggling Dataset Experiments.

Hyperparameter	NP	SP-MLP	SP-GRU
Sequence Encoder/Decoder			
Number of layers	2	2	1
Hidden dim	416	64	320
Partner Pooler $\psi(x_j)$			
Number of MLP layers	—	2	2
MLP hidden dim	—	64	64
Output dim	—	32	32
z Encoder			
Number of layers	2	2	2
Hidden dim	64	64	64
Representations			
e, r, s, z dim	64	64	64
Multi-Head Attention			
Query/Key dim	32	32	32
Number of heads	8	8	8
Number of parameters in -latent variant			
	2.8M	2.2M	3.0M

subset of the batch. Consequently, we further constrain samples in a batch to correspond to the same interacting group (see Section 2 for the underlying meta-learning intuition). For the same reason, we also ensure that a batch contains unique observed sequences, so that a single observed sequence does not dominate the aggregation of representations over context. This is because a single observed sequence has multiple associated future sequences at different offsets, and could show up multiple times in a batch through random sampling if not handled explicitly.

We optimize the models using Adam [77]. For the NP and SP-MLP models we use a batch size of 128, an initial learning rate of $3e-5$, and a weight decay of $5e-4$, and a dropout rate of 0.25. For the MLP-GRU models we use a batch size of 64, an initial learning rate of $1e-5$, and a weight decay of $1e-3$. The entire system was implemented using Pytorch [78] and Pytorch Lightning [79]. Every model was trained on a single NVIDIA GPU on an internal cluster depending on availability; one of Geforce GTX 970 (4 GB) or 1080 (8 GB), or Quadro P4000 (8 GB).

We validate the hyperparameters using 5-fold cross-validation, in the *random* context regime. At test, we use the same context sequences across models for fair comparison. The final model parameters for testing are obtained by averaging the parameters from the five best models during training. All testing was done with a batch size of 128 for consistency. All evaluation metrics are computed after destandardizing the location dimensions (orientation is already denoted by a unit quaternion, and therefore not standardized). The predicted std. deviations are scaled by the same value as the predicted means during destandardization.

D Additional Dataset Details

D.1 Synthesized Glancing Behavior Dataset

The set of pristine sinusoids representing the *Type I* glances is computed by evaluating the sine function at the bounds of 19 equally spaced partitions of $[0, 3\pi + \phi)$, for phase values ϕ in $[0, 2\pi)$ with a step size of 0.001. More concretely, this is the set

$$g = \{r : r = \sin(x), x = n \times (3\pi + \phi) / 19, n \in \{0, 1, \dots, 19\}, \phi = p \times 0.001, p \in \{0, 1, \dots, 6283\}\},$$

which results in 6284 sequences. The *Type III* glances are represented by identical sinusoids with clipped amplitudes for the last six timesteps, resulting in the final dataset of 12568 sequences. We train with batches of 100 sequences, using a randomly sampled 25 % of the batch as context. For evaluation, we fix 785 randomly sampled phase values as context for all models. For each phase, samples corresponding to both types of glances are included in the context set, effectively using 25 % of all samples as context at evaluation.

D.2 Preprocessing the Panoptic Haggling Dataset

We begin by converting the orientation normals into unit quaternions. While quaternions afford many benefits over other representations of rotation, their one downside is that they are not injective—the quaternion \mathbf{q} denotes an identical rotation to $-\mathbf{q}$. We address this by constraining every first quaternion of a sequence to the same hemisphere in quaternion space. To ensure smooth interpolation, the quaternion at every subsequent frame is chosen to be the one in $\{\mathbf{q}_t, -\mathbf{q}_t\}$ that is the shortest distance from \mathbf{q}_{t-1} along the unit hypersphere. As discussed in Section 5, we then split the interaction data into pairs of t_{obs} and t_{fut} windows to construct the samples for forecasting. Motivated by the domain focus on the organization of turn-taking, we consider window lengths of 2 seconds supported by dataset statistics and literature. The dataset duration of contiguous speech follows a mean of 2.13 s ($\sigma = 2.61$ s), which is close to the mean measure of 1.68 s found in turn-taking analysis [20, 80]. We generate sliding windows with an overlap of 0.8, constraining the offset between t_{obs} and t_{fut} to a maximum of 5 s. This is to roughly restrict candidate future windows to those starting after two turn changes. In total, we obtain about 140K observed-future sequence pairs for training, and about 40K pairs for testing. We standardize the location features to have zero mean and unit variance, using the train statistics to standardize the test sets.